

Microwave Wind Direction Retrieval over Antarctica

David G. Long and Mark Drinkwater
Brigham Young University Microwave Earth Remote Sensing Laboratory
459 Clyde Building, Provo, UT 84602
801-378-4383, FAX: 801-378-6586, e-mail: long@ee.byu.edu

Abstract—Over large regions of Antarctica, ice sheet and bedrock topography and the snow deposition, drift, and erosional environment combine to produce roughness on various scales. The roughness influences the microwave backscattering and emission properties of the surface, introducing azimuth-angle dependencies in the satellite observation data. In this paper we explore the use of data from SeaWinds on Quikscat, NSCAT, ERS AMI scatterometer mode, and SSM/I to study surface roughness effects in Antarctica. A simple empirical model for the azimuth variation in the radar backscatter is developed. Azimuthal variations in the data are highly correlated with the direction of the katabatic wind flow.

INTRODUCTION

Radiative cooling of surface air masses over the interior of Antarctica causes negative buoyancy and the air to sink downslope. As a result Antarctic ice sheet surface winds can maintain approximately the same speed and direction for weeks at a time. With these constant winds, sastrugi and snow drifts form aligned with the wind direction. Such erosional and depositional features are believed to be the dominant source of the previously observed azimuth variation in σ° [1].

We consider data from SeaWinds on QuikScat, the NASA scatterometer (NSCAT), the Wind Scatterometer mode (hereafter Escat) of the Advanced Microwave Instrument (AMI), and SSM/I data to study the microwave response over Antarctica. We examine the azimuthal variation in measurements of σ° and T_b to map the distribution of aligned surface roughness features and, hence, the wind direction. This study extends previous work and considers the influence of incidence-angle influence upon the magnitude of the azimuth modulations. A simple model is introduced which accounts for necessary first and second order terms, due to local slope and azimuth effects respectively. A more detailed analysis is presented in [2].

ANALYSIS

The Scatterometer Image Reconstruction (SIR) algorithm has been applied to generate enhanced resolution images from each sensor (see Figure 1). Because the NSCAT and Escat scatterometers make measurements over a range of incidence angles, the incidence angle dependence of σ° must be accounted for these sensors. For purposes of imaging, σ° (in dB) is modeled as a linear function of incidence angle θ , $\sigma^\circ(\theta) = \mathcal{A} + \mathcal{B}(\theta - 40^\circ)$, where \mathcal{A} is the σ° value at 40° (mid swath) incidence angle and \mathcal{B} describes the dependence of σ° on θ . For

SeaWinds and SSM/I, the \mathcal{A} images are backscatter or T_b at the nominal observation angle.

Based on subjective examination of the sensor images in Fig. 1, a number of study regions were selected for detailed analysis. Here we consider only a single region spanning 93° - 100° E and 73.5° - 74.5° S. This area has a mean slope of 1.34 m/km. Scatter plots of T_b and σ° versus relative azimuth angle over the sixteen day period between JD 268 and 283, 1996 are shown in Figs. 2 and 3. In these plots, measured values are shown as grey points. Individual measurements are binned into $\pm 3^\circ$ azimuth angle bins with the mean and the standard deviation indicated with a dark point and 1 sigma error bars.

In Fig. 2 SSM/I data exhibits a small azimuth angle range for this area but hints at a possible azimuth dependence on T_b . Some other regions show more conclusive azimuth dependence [2]. NSCAT data exhibits measurements at a number of essentially discrete azimuth angles, spread over the full 360° range. The Escat data also has discrete azimuth angles, but over a more limited range. These behaviors are typical of all the study areas considered. The NSCAT measurements clearly show modulation in the observed Ku-band σ° as a function of the azimuth angle. The more limited azimuth angle observations of the Escat data suggest a greater modulation at C-band but only from the NSCAT V pol data can a peak in the azimuth modulation (at approximately 5°) be determined with confidence. A second-order ($N = 2$) Fourier series (in azimuth angle, ϕ_i) is individually fit (in the least-squares sense) to each of the σ° versus azimuth angle scatter plots in these figures and is plotted as a solid curve.

Noting the dependence of σ° on incidence angle, we investigate the dependence of the azimuth modulation on incidence angle in NSCAT data with the aid of Fig. 3. In addition to the clear variation in the mean σ° with incidence angle, examination of these plots suggests that the modulation depth varies inversely with incidence angle, at least for V pol, and there appears to be negligible variation in the locations of the minima and maxima of the modulation as a function of incidence angle.

The asymmetric nature of the σ° modulation with azimuth angle suggests that both the first and second order terms are required to fit the data. To account for the variation in both incidence angle and azimuth angle, a simple empirical model is developed. Borrowing from ocean scattering theory, a simple second order harmonic model is assumed for the variation in σ° (in dB) with azimuth and incidence angles,

$$\sigma^\circ(\theta, \phi_i) = \mathcal{A} + \mathcal{B}(\theta - 40^\circ) + M_1 \cos(\phi_i + \phi_1) + M_2 \cos(2\phi_i + \phi_2)$$

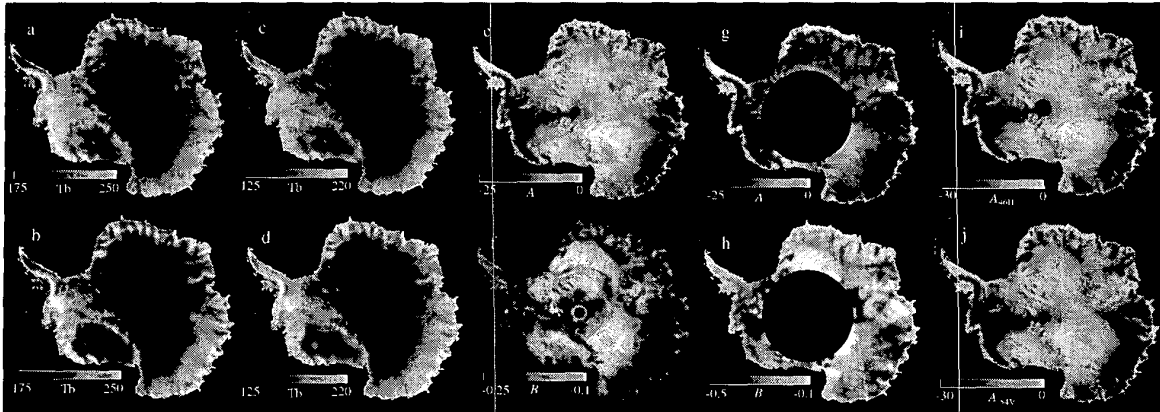


Figure 1: SSM/I-, NSCAT-, Escat-, and SeaWinds derived images of Antarctica produced with the aid of the SIR algorithm from six days of data (JD 277-282). (a) T_b at 19 GHz V pol. (b) T_b at 19 GHz H pol. (c) T_b at 37 GHz V pol. (d) T_b at 37 GHz H pol. (e) \mathcal{A} at 14 GHz V pol (f) \mathcal{B} at 14 GHz V pol. (g) \mathcal{A} at 5.3 GHz V pol (g) \mathcal{B} at 5.3 GHz V pol (h) SeaWinds H pol at 13.6 GHz (i) SeaWinds V pol at 13.6 GHz. NSCAT 14 GHz H pol \mathcal{A} and \mathcal{B} images are not shown. Image resolution reduced for comparison.

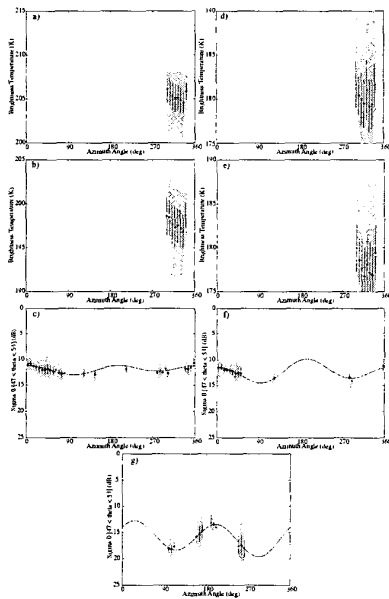


Figure 2: Scatter plots of T_B and σ^o versus azimuth angle. a) SSM/I 19v, d) SSM/I 19h, b) SSM/I 37v, e) SSM/I 37h, NSCAT c) V pol and f) H pol at 50° incidence angle, and g) Escat V pol at 50° incidence angle. The solid lines represent the second order azimuth fit (see text).

where \mathcal{A} and \mathcal{B} are defined as before; M_1 and M_2 are the magnitudes of the first-order and second-order azimuth angle harmonic terms, respectively; ϕ_1 and ϕ_2 are the phase angles of the first-order and second-order azimuth angle harmonic terms, respectively; and ϕ_i is the observation azimuth angle relative to north. As suggested by the plots in Fig. 3, M_1 and M_2 vary with incidence angle. Noting that the dependence of the az-

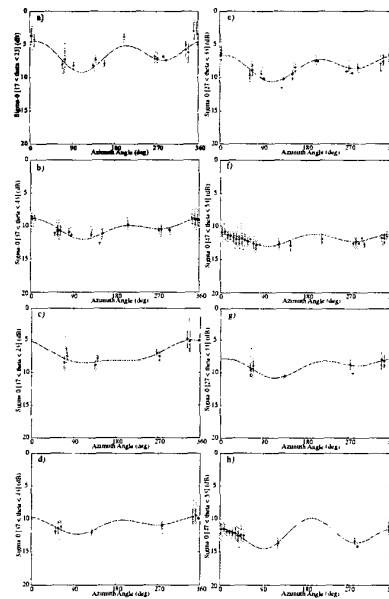


Figure 3: NSCAT σ^o versus azimuth angle at various incidence angles – V Pol (top four plots), H pol (bottom four plots). Measurements are from $\pm 3^\circ$ of the central incidence angles of 20° , 30° , 40° , and 50° . The solid lines represent the second order azimuth fit (see text).

imuth modulation depth in dB is often nearly linear with incidence angle, a very simple model for the dependence of M_1 and M_2 on incidence angle is, $M_1 = c_1 + d_1(\theta - 40^\circ)$ and $M_2 = c_2 + d_2(\theta - 40^\circ)$. Normalizing the incidence angle to 40° is done primarily for convenience.

To visualize $\sigma^o(\theta, \phi_i)$ at Ku-band, the model is fit to NSCAT V pol data and plotted in Fig. 4 for several study areas. We note

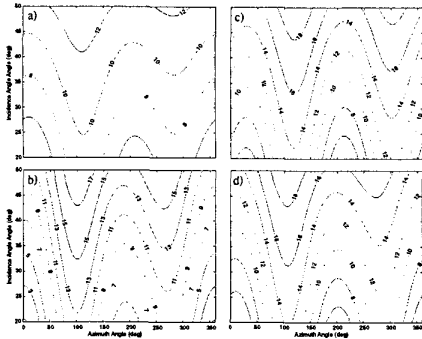


Figure 4: Contour plots of $\sigma^o(\theta, \phi_i)$ computed from the azimuth modulation model parameters estimated from V pol NSCAT data for several study areas.

a generally similar behavior in all regions. Over the ocean a similar behavior occurs but the highest ridge peak corresponds to the up-wind direction while the troughs correspond to the cross-wind direction. For Antarctic firn, the minimum of the backscatter versus azimuth direction generally corresponds to the wind direction, with some modification due to incidence angle effects. Since the local topographic slope and km-scale snow dunes modify the local incidence angle, the asymmetry in the modulated backscatter results from looking in the upslope and downslope direction. It is thus possible to unambiguously infer the wind direction from the σ^o measurements by locating the minima. However, since all that is needed is the location of the up-wind peak, a simplified model with constant incidence angle dependence can be used to evaluate the wind direction.

Using NSCAT data, the azimuth modulation can be evaluated over virtually the entire Antarctic continent on a fine scale using the simplified model. To compute the simplified model parameters, the SIR algorithm is first used to compute \mathcal{A} and \mathcal{B} images. Then, for each σ^o measurement, the forward projection is computed. The projection error is the difference between the forward projection and the measurement. For each pixel, the projection errors are accumulated and used to estimate the model parameters via least-squares.

Figure 5 presents NSCAT-derived images of the simplified model parameters. The azimuth angle harmonic magnitude images show significant coherent spatial variations in the azimuth modulation of σ^o . The crests of the ice divides separating the major wind and ice sheet drainage basins display the smallest standard deviations both before and after azimuth modulation removal. This, coupled with the extremely low magnitude values of the first- and second-order harmonic terms, is evidence for virtually no azimuth dependence along the divides. These also correspond with inflection lines in the \mathcal{A} and \mathcal{B} images, implying divides in the accumulation patterns and snow layering as a consequence of the topographically-influenced wind regime. These coupled observations imply lighter winds and lack of directionality in the wind direction (in these locations) with much smoother ice sheet surfaces and negligi-

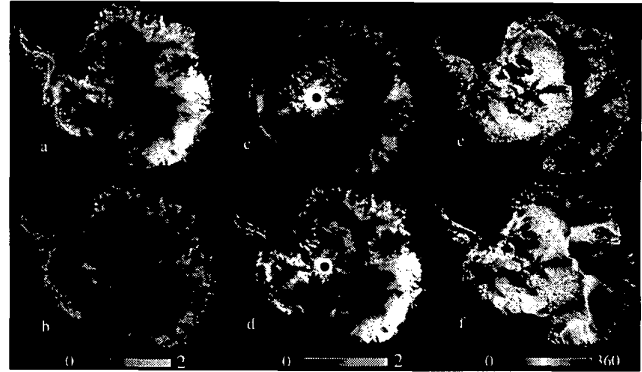


Figure 5: NSCAT images from six days (JD 277-282,1996) of v-pol data: a) projection error standard deviation prior to azimuth modulation removal, b) residual projection standard deviation after azimuth modulation estimation, c) magnitude (M_1) of the first-order azimuth modulation harmonic term, d) magnitude (M_2) of the second-order term, e) phase angle (ϕ_1) of the first-order term, f) angle (ϕ_2) of the second-order term.

ble aligned roughness, resulting in more isotropic backscatter. From these images the azimuth modulation minima can be located at each pixel location. Streamlines of these directions correspond closely with model-predicted katabatic winds [2].

CONCLUSION

These Antarctic observations clearly demonstrate that models of azimuthal variations in microwave data must account for both first- and second-order effects. Further studies are required to address the precise mechanisms which drive the observed signatures. While it is clear that the wind causes roughness in the bedding structure and annual layering of accumulated and wind-redistributed snow, it is not clear why alignments ought to be coherent with depth, though coherent internal reflections may play a role. Microwave backscatter at different frequencies can be exploited to discriminate between physical properties of the snow and firn at varying depths and address open questions regarding the links between the firn layer characteristics, wind-induced bedding structures, and the thermodynamic processes linking these physical attributes to the atmospheric conditions on the ice sheet [2].

REFERENCES

- [1] Remy, F., M. Ledroit, and J.F. Minster, "Katabatic Wind Intensity and Direction over Antarctica Derived from Scatterometer Data," *Geophysical Research Letters*, Vol. 19, pp. 1021-1024, 1992.
- [2] Long, D.G., and M.R. Drinkwater, "Azimuth Variation in Microwave Scatterometer and Radiometer Data Over Antarctica," to appear, *IEEE Trans. Geosci. Remote Sens.*, 2000.